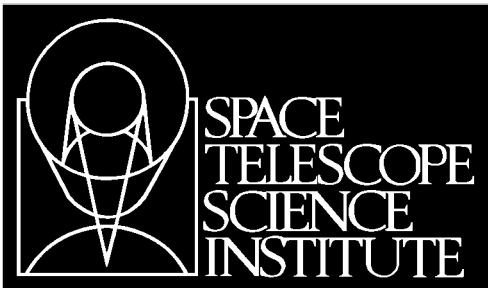


Space Telescope Science Institute
James Webb Space Telescope Mission

Further Comparisons of Super-Sky and Self-Calibration Flat Fields for Simulated Mid-Infrared JWST Images

18 April 2003

Issue A



REVISION HISTORY

ISSUE	DESCRIPTION	DATE
A	Initial Release	18-Apr-03

James Webb Space Telescope Mission

Further Comparisons of Super-Sky and Self-Calibration Flat Fields
for Simulated Mid-Infrared JWST Images

April 18, 2003

PREPARED BY:	<u>Sherie T. Holfeltz</u> NAME	<u>Instruments</u> ORG.
	_____ SIGNATURE	_____ DATE
	<u>Stefano Casertano</u> NAME	<u>Instruments</u> ORG.
	_____ SIGNATURE	_____ DATE

APPROVED BY: _____
SIGNATURE

NAME

TITLE

Further Comparisons of Super-Sky and Self-Calibration Flat Fields for Simulated Mid-Infrared JWST Images

S. T. Holfeltz and S. Casertano
April 18, 2003

ABSTRACT

Self-calibration flat fields are compared to super-sky flat fields for simulated JWST images in this report which is a continuation of the investigation presented in Casertano & Holfeltz 2002. Self-calibration flats derived from 10 or 100 dithered exposures with a combined exposure time of 100 ksec typically result in flat fields which are good to approximately 1% at 2 microns and 0.03% at 20 microns. Super-sky flats derived from 10-100 chopped or dithered exposures totalling 100 ksec exposure time yield flats good to 1.6% at 2 microns and 0.04% at 20 microns. Dithering the science data was found to be crucial in obtaining satisfactory calibrations, regardless of the provenance of the applied flat field. Both methods come within 20% of the results expected for a perfect flat field without especially aggressive observation planning, as long as proper dithering is used.

Introduction

The science goals of the James Webb Space Telescope (JWST) require the detection and measurement of small faint sources down to 10^{-4} of the sky brightness for the most challenging observations, and typically $2 - 5 \times 10^{-4}$. This will likely require the subtraction of the background and knowledge of the flat field with a typical accuracy of $10^{-4} - 10^{-5}$ on spatial scales ranging from a single pixel to the full field of view. This report presents the results of simulations designed to achieve a shot noise per pixel of 1% at 2 microns and 0.03% at 20 microns. We compare the efficacy of two different flat fielding techniques for JWST observations: the super-sky flat and self-calibration methods.

The Super-Sky Flat & Self-Calibration Methods

The super-sky flat method is designed to elicit the detector response function and potentially variable sky level by combining source-free regions of many different images, scaled to a common sky level. The synthetic sky thus constructed is then scaled and subtracted from each image. If the underlying true sky is featureless, the sky image thus constructed is also a measurement of the detector response, and can be used as an inverse flat field - a *super-sky flat*, at least for sources that have the same color as the sky.

The assumptions underlying this technique are that the sky has the same shape in all images (although the overall level may vary) and that sources can be successfully identified and rejected when comparing a sufficient number of images at different pointings. It is expected that for JWST, temporal variations in both sky level and shape will most likely be very small, except possibly for the background contribution from the telescope itself. However, sources at a significant level may cover a large percentage of JWST images, because of lower sky level, higher desired sensitivity, and longer integrations at each pointing; consequently, careful source filtering may be required.

The *self-calibration method* (Fixsen et al. 2000, Arendt et al. 2000), uses dithered observations to solve for the flat field by comparing the signals measured when the same sky position is observed in different detector pixels. This method assumes that the brightness at each location is constant in time. The self-calibration solutions for the simulations presented here were obtained using an iterative method developed by one of us (SC).

Each technique exhibits characteristics and advantages over the alternative method under different circumstances; a closer examination of the differences between the two methods under consideration is useful.

- The self-calibration method can be used even if the image is filled with sources. The super-sky flat method requires the successful filtering out and rejection of sources over the entire field of view.
- The self-calibration method is more efficient in terms of signal-to-noise, since it uses all detector pixels, regardless of whether they contain a source or not. With the super-sky flat method, pixels identified as containing sources (which contain more flux than source-free pixels) are excluded from the solution.
- With the self-calibration method, the sky can be flat-fielded and subtracted from the data obtained for a single program, providing some protection against changes in the sky and flat field properties. Super-sky flats require disparate pointings; the accompanying increased slew time leads to an increased probability of changes in the both the sky and flat field properties over the course of the requisite observations. The independent pointing requirements of the super-sky flat method will automatically be fulfilled by the routine execution of science and/or calibration observations.

- The super-sky flat is sensitive to gradients in the sky on the scale of the detector field of view. Any significant variations of the background signal within the field of view will cause an incorrect estimate of the flat field. Such variations are expected to be very small on the scale of the NIRCcam field of view, but their impact needs to be quantified.
- The self-calibration method is ideally suited for dithered data (exposure-to-exposure offsets smaller than the field of view), thus avoiding large slews that might introduce changes in the sky pattern. The super-sky method performs best with chopped data (exposure-to-exposure offsets larger than the size of the largest source) which are less likely than dithered data to contain pixels for which there exist no source-free observations.
- The self-calibration method is more sensitive than the super-sky flat method to image imperfections such as geometric distortion, subpixelation of sources, and variations in the point-spread function over the field of view.
- Self-calibration yields tightly constrained calibrations for those pixels which have observed a common region of sky, while the relative calibration of pixels which have not imaged a common sky region are constrained indirectly by nearby pixels which have observed common sky regions. This can lead to non-trivial covariance between pixels that are not closely connected. Consequently, the spacing and regularity of the dither pattern may affect the quality of the derived flat field. Super-sky flats require only that each pixel falls at least once in a source-free region.
- Self-calibration is computationally more intensive than the super-sky flat method, especially for the large-format images expected from NIRCcam.

Previous Investigations

CH02 included simulations at 10, 20, and 28 microns, with exposure times of 25 ksec per exposure. Dithered datasets included 50-100 positions, resulting in a cumulative exposure time of 1250 - 2500 ksec per dataset. The self-calibration flats were derived from dithered data only and the super-sky flats were constructed only from chopped data. The plate scale was 0.3 arcsec/pixel at all wavelengths, and the full width at half maximum of the point spread function was taken to be 1.4, 2.8, and 3.8 pixels at 10 μm , 20 μm , and 28 μm , respectively. The following nearly ideal conditions were adopted in CH02:

- The only “imperfections” in the images were the true flat field and a level of noise consistent with the detector characteristics of JWST.
- The simulated images took into account the expected distribution of sources at JWST sensitivity, as well as the expected properties of JWST instruments and detectors at the selected wavelengths.
- The simulated images were an idealized representation of the sky, with gain variable from pixel to pixel but constant in time and with noise that followed a well-defined model.
- We assumed that all other imperfections, such as non-linearity, saturation, bias fluctuations, cosmic rays and so on were perfectly removed by the standard calibration.

- The true sky was always flat, and thus flat-fielding the data was necessary and sufficient for sky subtraction.

Given the simplifying assumptions adopted, both the self-calibration and super-sky flat fielding methods were found to be capable of producing flat fields that satisfy the JWST science requirements, provided that the instrumental response and background properties remain constant on timescales of ~ 1 month.

Current Investigation

For the current study, we adopted all of the simplifying assumptions outlined above, but we considered more realistic observing scenarios, designed so as to allow a direct comparison between the two methods. The wavelengths chosen for the current study were $2\ \mu\text{m}$ and $20\ \mu\text{m}$. Plate scales of $0.035\ \text{arcsec/pixel}$ and $0.100\ \text{arcsec/pixel}$ were used at $2\ \mu\text{m}$ and $20\ \mu\text{m}$, respectively. The full width at half maximum of the point spread function was taken to be 2.4 pixels at $2\ \mu\text{m}$ and 8.4 pixels at $20\ \mu\text{m}$. Exposure times include 1 ksec, 5 ksec, 10 ksec, and 100 ksec per exposure. The total exposure time per dataset was held fixed at 100 ksec; datasets consist of one hundred 1 ksec exposures, twenty 5 ksec exposures, or ten 10 ksec exposures. Both dithered and chopped data were included. The self-calibration method was applied only to dithered datasets; the super-sky flat technique was used on both dithered and chopped datasets.

Below we examine, in turn, the composition of the “truth images”, the construction of the observed images from the truth images, and the derivation & application of the flat fields. Next, the metrics selected to assess the relative success of the two techniques are described and the results presented. Finally, the conclusions drawn from the current study are summarized.

Truth Images

There are two different types of “truth images” to consider: the simulated sky and the true flat field.

Simulated Sky

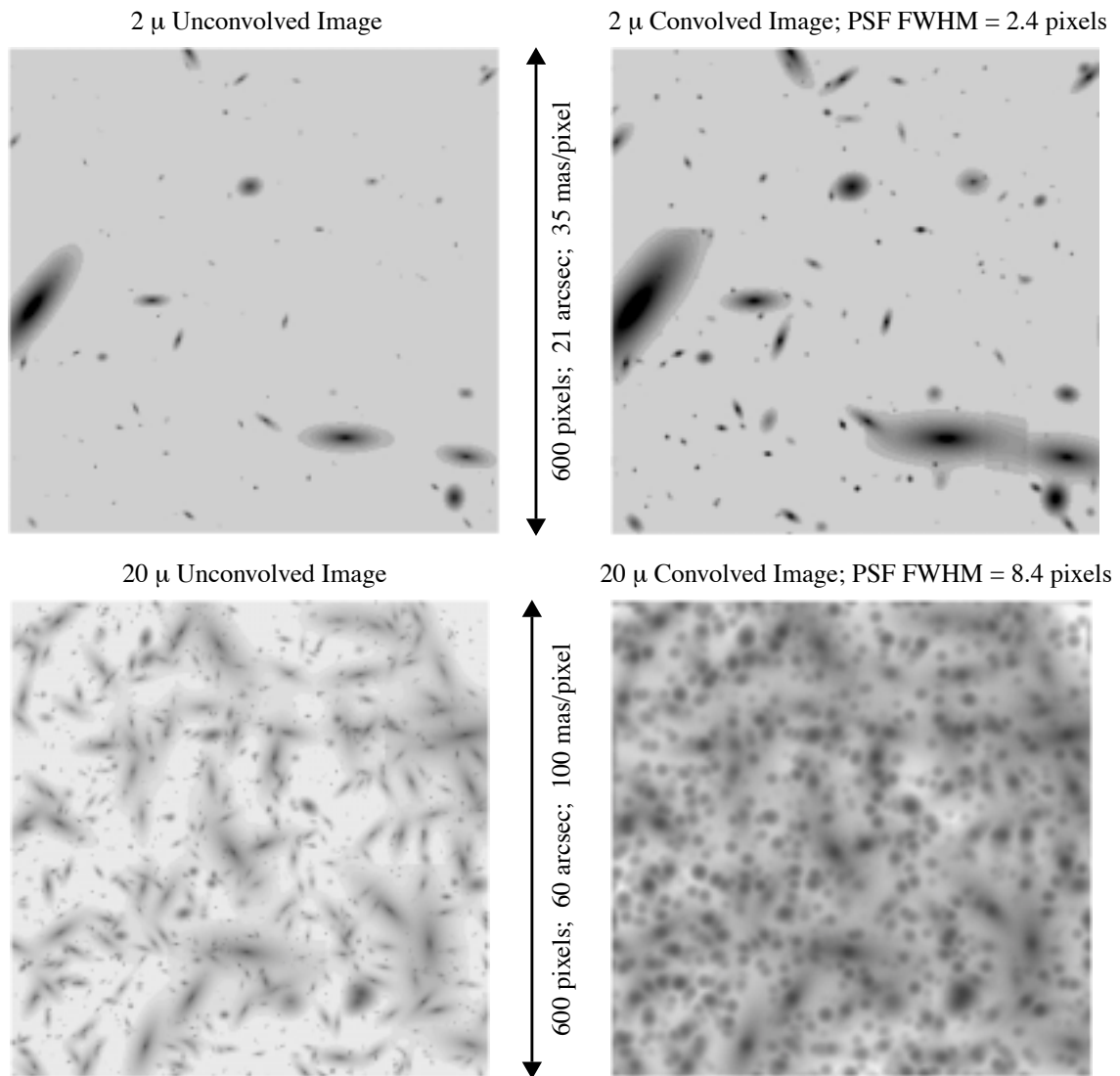
The simulated sky images were produced using IDL code written by E. Morse, which originally included the following noise components: self emissivity, dark current, read noise, zodiacal background, and Poisson shot noise. For this investigation, the code was modified slightly to not add the read noise and shot noise; noise due to these sources was generated by downstream software and added to the individual exposures of the simulated sky.

The sky images were 600×600 pixels. Independent simulated were generated at wavelengths of 2 microns and 20 microns, each with a spectral resolution of 5. The pixel scales at 2 and 20 microns were taken to be 35 and 100 milli arcseconds per pixel respectively. The FWHM of the PSFs with which the simulated sky images were convolved were 2.4 pixels at 2 microns and 8.4 pixels at 20 microns. The count rates for the 20 micron data are approximately 1400 times the count rates for the 2 micron data. The characteristics of the simulated sky images are given in Table 1 below. Simulated 600×600 pixel sky images for 100 ksec exposure time at 2 microns and 20 microns are shown in Figure 1. The truncated edges on the large galaxies in Figure 1, especially apparent in the 2 micron simulations, are due to the finite box size employed by the IDL simulation code when generating sources.

Table 1. Summary of Simulated Sky Images

Wavelength (microns)	Pixel Scale (mas)	Exp. Time (ksec)	PSF FWHM (pixels)	Mean Counts Image Conv'd with PSF	Total Counts Image Conv'd with PSF
2	35	1	2.4	100	3.76211e+07
2	35	5	2.4	480	1.75937e+08
2	35	10	2.4	973	3.54345e+08
2	35	100	2.4	11715	4.06842e+09
20	100	1	8.4	139934	5.02618e+10
20	100	5	8.4	699688	2.52516e+11
20	100	10	8.4	1399000	5.05011e+11
20	100	100	8.4	13990000	5.03509e+12

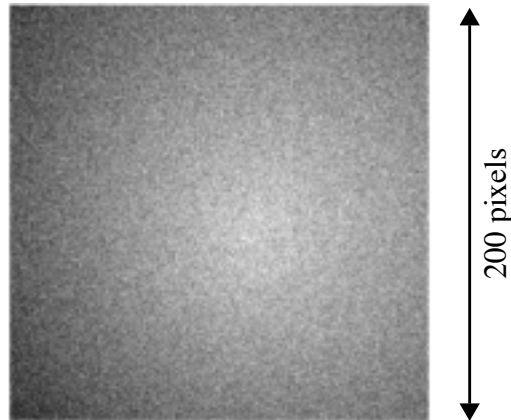
Figure 1: Simulated unconvolved and PSF-convolved 100 ksec sky images at 2 microns and 20 microns; the two images represent different regions of the sky.



True Flat Field

The “true” flat field, shown in Figure 2, was kept constant throughout the calculations. It was designed to include a dome-like feature as well as 2-dimensional second order polynomial fluctuations and pixel to pixel variations. The large-scale features produce a $\sim 20\%$ peak-to-peak variation in sensitivity, while the pixel to pixel variations are on the order of 2%-3%. The overall standard deviation is 0.04519; the mean is 1.000. The minimum and maximum values are, respectively, 0.8078 and 1.152.

Figure 2: “True” Flat Field



Observed Data

Simulated data include self emissivity, dark current, and zodiacal background and do not include read noise, Poisson noise, or flat field. Observed data are obtained from simulated data by adding noise and applying the true flat field as outlined below.

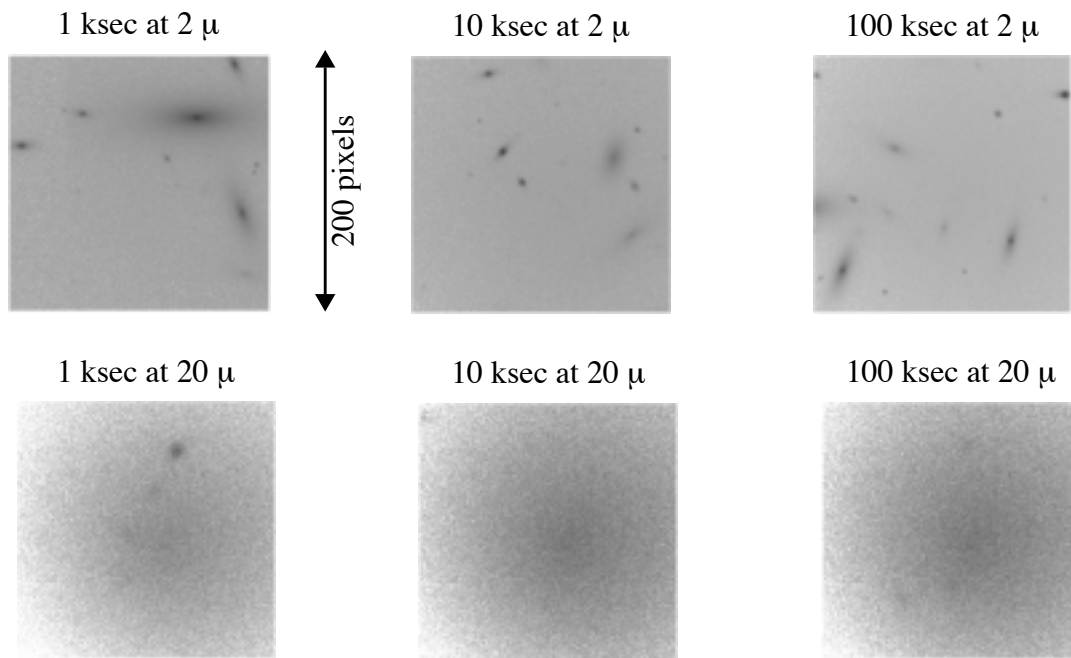
A 200×200 pixel region of a simulated, convolved sky image was extracted as the starting point of each observation. The true flat field was applied to each observation followed by the addition of read noise (3 counts at 2 microns, 30 counts at 20 microns), and the pseudo-Poissonian shot noise, generated by multiplying a Gaussian distribution by the square root of the signal. This procedure results in self emissivity, dark current, and zodiacal background which may vary from one sky simulation to another but which remain constant within a given dither pattern, and read noise and shot noise which vary from exposure to exposure within the dither pattern. Observations thus obtained were used to build flat fields and serve as science data to be calibrated by said flat fields.

Science Data

Five science datasets were defined, ranging in the number of exposures from 1 to 100 and with a constant total exposure time of 100 ksec. The science data included one single-pointing exposure, 2 spirally dithered and 2 randomly dithered patterns. The mean and standard deviation of each science dataset are summarized in Table 2. Individual frames from the simulated science observations are shown in Figure 3. At 20 microns, the variation in the sky due to the flat field is often larger than the signal from the simulated sources.

Table 2. Statistical Properties of Science Observation Datasets

Science Dataset	2 microns		20 microns	
	Mean	σ	Mean	σ
1 × 100-ksec exposure	9879	8649	1.400E7	633257
10 × 10-ksec random dither exposures	972	565	1.400E6	63024
10 × 10-ksec spiral dither exposures	980	588	1.400E6	63310
100 × 1-ksec random dither exposures	130	190	1.401E5	6459
100 × 1-ksec spiral dither exposures	130	193	1.401E5	6491

Figure 3: Simulated science observations, including flat field, read noise, and shot noise.***Flat Field Data***

The following four dithered science observation datasets were conscripted as self-calibration flat datasets:

- 10 position, 10 ksec per position random dither
- 10 position, 10 ksec per position spiral dither
- 100 position, 1 ksec per position random
- 100 position, 1 ksec per position spiral dither.

The following science observation datasets were designated as super-sky flat datasets:

- 10 position, 10 ksec per position random dither
- 10 position, 10 ksec per position spiral dither
- 20 chopped pointings, 5 ksec per pointing

- 100 position, 1 ksec per position random dither
- 100 position, 1 ksec per position spiral dither
- 100 chopped pointings, 1 ksec per pointing

Construction & Application of Flat Fields

Sixty-four different flat fields were constructed: 4 self-calibration flats and 28 super-sky flats at each of the two wavelengths under investigation. Both the self-calibration and super-sky flats containing dithered data are composed of the same science datasets, for clarity in comparison. The same science datasets which went into the construction of the flat fields were also used to measure the efficacy of the derived flats in calibrating science observations. Chopped observations were used only for the derivation of super-sky flats.

Self-Calibration Flats

The self-calibration datasets identified above were used as input data for the self-calibration software which iteratively solved for the flat field and the sky. The iterative solution starts from a perfectly uniform flat field and constant sky. The current model is used to predict the observations; the difference between predicted and observed data is used to improve the current guesses, so that eventually the method converges to a final best-fit for both sky and flat field.

Super-Sky Flats

The super-sky flat method utilizes iterative sigma clipping to combine several observations of the sky, rejecting those pixels which contain sources, and averaging over those pixels which are within a 3σ or 5σ threshold from the median image. The sigma clipping algorithm used herein differs from that used previously (in CH02). Previously, the median flats were clipped with respect to the median image and the mean flats were clipped with respect to the mean image. The median was found to be a much better discriminator for identifying sources and rejecting pixels than the mean (CH02). For this study, the sigma clipping threshold was defined relative to the median, regardless of whether the final averaging was the mean or the median.

Super-sky flats were constructed from both dithered and chopped data, as described above. Each simulated sky exposure was stamped with the true flat field response, then read noise (3 counts for 2 micron data, 30 counts for 20 micron data) and shot noise was added; finally, each observation was divided by its median value. Outliers beyond the 3σ or 5σ threshold from the median image were iteratively clipped. The unrejected pixels were then averaged, using either the mean or the median, for the final derived super-sky flat field.

Calibrating the Science Datasets

Each science dataset was calibrated with each derived flat field of the appropriate wavelength in turn, by dividing the flat field into the observed data. Dithered data were then shifted and coadded; the final calibrated mosaic images consist of the mean of the coadded data.

Assessing The Efficacy of the Derived Flat Fields

Three separate metrics have been defined and calculated to help assess the relative efficacy of the flat fields derived from the two different techniques in question.

Flat Metric

The *flat metric* was designed to measure how good each derived (fitted) flat field was, i.e., how much it differed from the true flat field. The flat metric is defined as $\sigma(\text{scaled fitted flat} - \text{true flat})$ where the scaled fitted flat is the derived flat divided by the mean of the ratio of the derived flat to the true flat:

$$\text{scaled fitted flat} = \text{fitted flat} / \langle \text{fitted flat} / \text{true flat} \rangle.$$

The flat metrics are given for each of the derived flats plus the true flat, in Table 3 below. The flat field with the best (smallest) flat metric for each dataset is highlighted. In all cases for which there exist self-calibration flats, the self-calibration flats provide a better fit to the true flat than the super-sky flats, as measured by the flat metric. The 20 micron flats are approximately 10 times better than the 2 micron flats (due to larger count rates); however, one must recall that the sky needs to be subtracted much better at longer wavelengths. The poor flat metric obtained for the 2 micron 100×1 ksec random dither super-sky flat was due to a relatively large, bright galaxy which was dithered predominantly in one quadrant of the detector, resulting in residual signal in the final image. The self-calibration method performed much better on the same dataset.

Table 3. Flat Metrics For Derived Scaled Flat Fields

Flat Observations	Flat Metric = $\sigma(\text{scaled fitted flat} - \text{true flat})$				
	Self-Cal	3σ mean	3σ median	5σ mean	5σ median
2 microns					
10 × 10 ksec random dither	0.0116047	0.0150147	0.0157214	0.0150232	0.0157627
10 × 10 ksec spiral dither	0.0114929	0.0184918	0.0185295	0.0185301	0.0186445
10 × 10 ksec chopped	N/A	0.0182309	0.0176535	0.0181508	0.0178499
20 × 5 ksec chopped	N/A	0.0126896	0.0144350	0.0126868	0.0142838
100 × 1 ksec random dither	0.0100189	0.1043220	0.0943850	0.1040210	0.0940241
100 × 1 ksec spiral dither	0.0102145	0.0186547	0.0192652	0.0187637	0.0190937
100 × 1 ksec chopped	N/A	0.0136200	0.0150805	0.0135662	0.0150524
20 microns					
10 × 10 ksec random dither	0.000305088	0.000380170	0.000401676	0.000375110	0.000401821
10 × 10 ksec spiral dither	0.000312634	0.000380876	0.000398818	0.000377796	0.000399622
10 × 10 ksec chopped	N/A	0.000393588	0.000406594	0.000391498	0.000409364
20 × 5 ksec chopped	N/A	0.000359574	0.000391744	0.000359129	0.000392881
100 × 1 ksec random dither	0.000279348	0.000589249	0.000556444	0.000583197	0.000559330
100 × 1 ksec spiral dither	0.000275216	0.000295650	0.000357569	0.000295268	0.000359720
100 × 1 ksec chopped	N/A	0.000306391	0.000363967	0.000305806	0.000363872

Sky Metric

The efficacy of the derived flat fields, as applied to the science data, was measured via the *sky metric* which is defined as $\sigma(\text{scaled fitted sky counts per 100 ksec} - \text{true sky counts per 100 ksec})$. Sky metrics for the calibrated 2 micron and 20 micron data are shown in Table 4 and Table 5, respectively. The best sky metric for each science dataset at each wavelength is highlighted in the table. At 2 microns, the self-calibration flats provided the best fit of the observed data to the true data for all 5 science datasets. At 20 microns, 4 of the 5 best fits were from self-calibration and one was from a super-sky flat.

The sky metrics presented in the tables were calculated using sky pixels with cumulative exposure times of 100 ksec except for the 100 × 1 ksec spiral dithered science dataset which uses sky pixels with exposure times greater than or equal to 60 ksec. Figure 4 and Figure 5 plot the sky metric of a calibrated science dataset vs. the flat metric of the flat field used in the calibration. It is clear that dithered science observations result in better (lower) sky metrics than undithered data for a given flat field. The outlier points in Figure 4 are due to the poor flat fields resulting from the 2 micron 100 × 1 ksec random dither super-sky flat; one can see that even for relatively poor flat fields, dithering the science data is helpful.

Noise Metric

The noise characteristics of the calibrated science data are also of interest. A *noise metric*, to measure the ratio of the measured noise to the expected noise, may be defined as:

$$\alpha = \sqrt{\frac{\langle (\text{fitted sky} - \text{true sky})^2 / (\text{estimated noise})^4 \rangle}{\langle 1.0 / (\text{estimated noise})^2 \rangle}}$$

where the estimated noise is defined as follows:

$$\text{estimated noise} = \sqrt{(\text{fitted sky} + \text{readnoise}^2) / (\# \text{ of valid observations})}.$$

Table 6 and Table 7 present the noise metrics for the 2 micron and 20 micron data. The best sky metric for each science dataset is highlighted. At 2 microns, 4 of the 5 best noise metrics were provided by the self-calibration flats; the fifth was a super-sky flat. At 20 microns, all of the best noise solutions were from super-sky flats.

Noise metrics were calculated using sky pixels with cumulative exposure times of 100 ksec except for the 100 × 1 ksec spiral dithered science dataset which uses sky pixels with exposure times greater than or equal to 60 ksec. Figure 6 and Figure 7 plot the noise metric of a calibrated science dataset as a function of the flat metric of the applied flat field. Dithered science observations resulted in better (lower) noise metrics than undithered data for a given flat field. The outlier points in Figure 4 are due to the poor flat fields, affected by the large galaxy, resulting from the 2 micron 100 × 1 ksec random dither super-sky flat.

Table 4. Sky metrics for 2 micron science datasets as a function of applied flat field.

Characteristics of Applied Flat Field		2 micron Science Data Sky Metric				
Flat Type	Flat Data	^a No Dither 1 × 100ksec	^b Random 10 × 10ksec	^c Spiral 10 × 10ksec	^d Random 100 × 1ksec	^e Spiral 100 × 1ksec
true flat	N/A	100.399	99.530	99.021	106.370	167.830
self-calibration	10 × 10 ksec random dither	181.717	109.559	107.883	106.934	171.464
self-calibration	10 × 10 ksec spiral dither	176.213	107.585	112.929	107.138	173.552
self-calibration	100 × 1 ksec random dither	174.836	107.668	106.136	107.382	169.884
self-calibration	100 × 1 ksec spiral dither	166.327	106.329	105.581	107.329	170.125
3σ mean super-sky	10 × 10 ksec random dither	195.206	119.335	140.440	108.485	173.731
3σ mean super-sky	10 × 10 ksec spiral dither	248.511	146.439	168.767	109.968	175.292
3σ mean super-sky	10 × 10 ksec chopped	306.747	198.218	189.979	117.798	171.381
3σ mean super-sky	20 × 5 ksec chopped	184.234	121.895	115.800	111.009	173.626
3σ mean super-sky	100 × 1 ksec random dither	1176.490	758.464	734.029	721.205	218.607
3σ mean super-sky	100 × 1 ksec spiral dither	254.737	142.250	143.889	134.254	178.126
3σ mean super-sky	100 × 1 ksec chopped	214.276	128.759	133.353	107.904	172.396
3σ median super-sky	10 × 10 ksec random dither	224.892	129.444	130.273	108.269	177.153
3σ median super-sky	10 × 10 ksec spiral dither	247.596	143.699	150.520	109.751	177.835
3σ median super-sky	10 × 10 ksec chopped	272.133	181.603	172.421	112.931	174.209
3σ median super-sky	20 × 5 ksec chopped	209.714	126.827	117.688	110.660	172.545
3σ median super-sky	100 × 1 ksec random dither	1004.620	667.688	646.937	629.703	205.338
3σ median super-sky	100 × 1 ksec spiral dither	253.337	150.986	142.435	129.081	175.228
3σ median super-sky	100 × 1 ksec chopped	230.319	124.366	127.266	107.945	172.420
5σ mean super-sky	10 × 10 ksec random dither	201.175	116.578	133.144	108.130	172.364
5σ mean super-sky	10 × 10 ksec spiral dither	231.420	137.676	153.776	110.324	174.802
5σ mean super-sky	10 × 10 ksec chopped	311.179	209.722	184.609	116.974	172.261
5σ mean super-sky	20 × 5 ksec chopped	205.562	119.065	120.134	111.513	170.585
5σ mean super-sky	100 × 1 ksec random dither	1201.190	761.204	733.472	719.098	219.579
5σ mean super-sky	100 × 1 ksec spiral dither	243.851	153.145	142.037	134.619	177.917
5σ mean super-sky	100 × 1 ksec chopped	216.983	123.628	126.085	108.247	171.586
5σ median super-sky	10 × 10 ksec random dither	216.654	122.587	126.470	108.348	170.194
5σ median super-sky	10 × 10 ksec spiral dither	242.527	139.243	180.729	109.780	173.494
5σ median super-sky	10 × 10 ksec chopped	296.886	183.190	165.570	113.696	169.848
5σ median super-sky	20 × 5 ksec chopped	197.661	116.153	113.810	110.831	172.593
5σ median super-sky	100 × 1 ksec random dither	1062.950	666.311	643.336	627.754	206.449
5σ median super-sky	100 × 1 ksec spiral dither	254.875	155.675	150.352	128.669	174.312
5σ median super-sky	100 × 1 ksec chopped	246.005	120.075	119.277	108.161	172.815

^a Includes all 40,000 sky pixels, each with a cumulative exposure time of 100 ksec.

^b Includes 16,157 sky pixels, each with a cumulative exposure time of 100 ksec.

^c Includes 18,422 sky pixels, each with a cumulative exposure time of 100 ksec.

^d Includes 6,141 sky pixels, each with a cumulative exposure time of 100 ksec.

^e Includes 4,967 sky pixels, each with a cumulative exposure time of 60 ksec.

Table 5. Sky metrics for 20 micron science datasets as a function of applied flat field.

Characteristics of Applied Flat Field		20 micron Science Data Sky Metric				
Flat Type	Flat Data	^a No Dither 1 × 100ksec	^b Random 10 × 10ksec	^c Spiral 10 × 10ksec	^d Random 100 × 1ksec	^e Spiral 100 × 1ksec
true flat	N/A	3752.74	3739.26	3680.13	3663.94	4769.47
self-calibration	10 × 10 ksec random dither	5716.71	3992.72	3907.55	3688.97	4796.28
self-calibration	10 × 10 ksec spiral dither	5785.98	3972.28	4134.68	3674.97	4880.17
self-calibration	100 × 1 ksec random dither	5402.41	3979.94	3919.49	3704.59	4796.21
self-calibration	100 × 1 ksec spiral dither	5409.26	3933.63	3872.17	3685.32	4797.68
3σ mean super-sky	10 × 10 ksec random dither	6516.34	4461.64	4358.07	3882.34	4813.91
3σ mean super-sky	10 × 10 ksec spiral dither	6536.86	4267.78	4528.39	3864.50	4829.32
3σ mean super-sky	10 × 10 ksec chopped	6665.45	4209.18	4295.00	3810.35	4819.36
3σ mean super-sky	20 × 5 ksec chopped	6230.46	4134.76	4072.22	3705.06	4794.72
3σ mean super-sky	100 × 1 ksec random dither	8922.73	6207.71	5518.83	4970.61	4805.31
3σ mean super-sky	100 × 1 ksec spiral dither	5597.62	3958.77	3976.15	3689.35	4824.89
3σ mean super-sky	100 × 1 ksec chopped	5705.83	3960.75	3947.51	3707.39	4784.47
3σ median super-sky	10 × 10 ksec random dither	6762.20	4387.09	4298.27	3831.51	4824.24
3σ median super-sky	10 × 10 ksec spiral dither	6734.65	4287.56	4400.63	3819.73	4817.79
3σ median super-sky	10 × 10 ksec chopped	6816.31	4212.13	4249.43	3774.94	4809.48
3σ median super-sky	20 × 5 ksec chopped	6625.07	4137.16	4093.83	3711.65	4795.94
3σ median super-sky	100 × 1 ksec random dither	8531.92	5677.20	5178.86	4629.04	4816.12
3σ median super-sky	100 × 1 ksec spiral dither	6252.69	4070.18	4091.87	3708.62	4817.31
3σ median super-sky	100 × 1 ksec chopped	6322.42	4082.73	4006.27	3712.16	4814.93
5σ mean super-sky	10 × 10 ksec random dither	6463.80	4427.32	4318.64	3867.96	4823.26
5σ mean super-sky	10 × 10 ksec spiral dither	6515.38	4256.69	4496.01	3855.24	4823.05
5σ mean super-sky	10 × 10 ksec chopped	6622.68	4201.46	4290.82	3806.05	4801.82
5σ mean super-sky	20 × 5 ksec chopped	6247.06	4133.95	4081.07	3699.05	4794.00
5σ mean super-sky	100 × 1 ksec random dither	8847.62	6163.42	5489.14	4936.33	4797.23
5σ mean super-sky	100 × 1 ksec spiral dither	5608.59	3960.93	3966.58	3693.55	4824.35
5σ mean super-sky	100 × 1 ksec chopped	5697.57	3963.82	3936.83	3708.58	4804.47
5σ median super-sky	10 × 10 ksec random dither	6776.49	4398.43	4308.80	3824.63	4823.58
5σ median super-sky	10 × 10 ksec spiral dither	6735.56	4245.55	4374.75	3820.90	4809.54
5σ median super-sky	10 × 10 ksec chopped	6838.14	4227.39	4268.98	3781.12	4815.25
5σ median super-sky	20 × 5 ksec chopped	6639.28	4130.36	4125.64	3714.08	4806.64
5σ median super-sky	100 × 1 ksec random dither	8567.44	5724.22	5183.16	4674.06	4809.15
5σ median super-sky	100 × 1 ksec spiral dither	6298.67	4061.38	4055.89	3707.35	4805.85
5σ median super-sky	100 × 1 ksec chopped	6306.88	4043.44	4020.49	3712.32	4795.55

^a Includes all 40,000 sky pixels, each with a cumulative exposure time of 100 ksec.

^b Includes 13,189 sky pixels, each with a cumulative exposure time of 100 ksec.

^c Includes 18,476 sky pixels, each with a cumulative exposure time of 100 ksec.

^d Includes 5,427 sky pixels, each with a cumulative exposure time of 100 ksec.

^e Includes 4,889 sky pixels, each with a cumulative exposure time of 60 ksec.

Figure 4: Flat metric vs. sky metric for 2 micron science datasets.

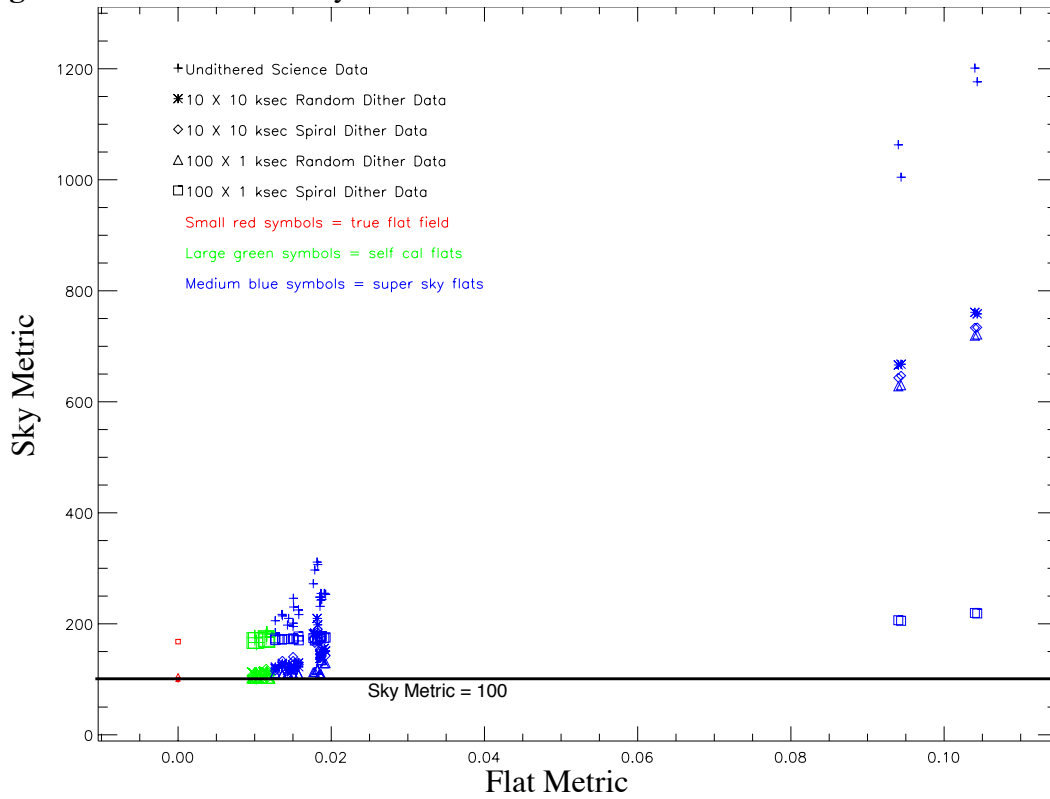


Figure 5: Flat metric vs. sky metric for 20 micron science datasets.

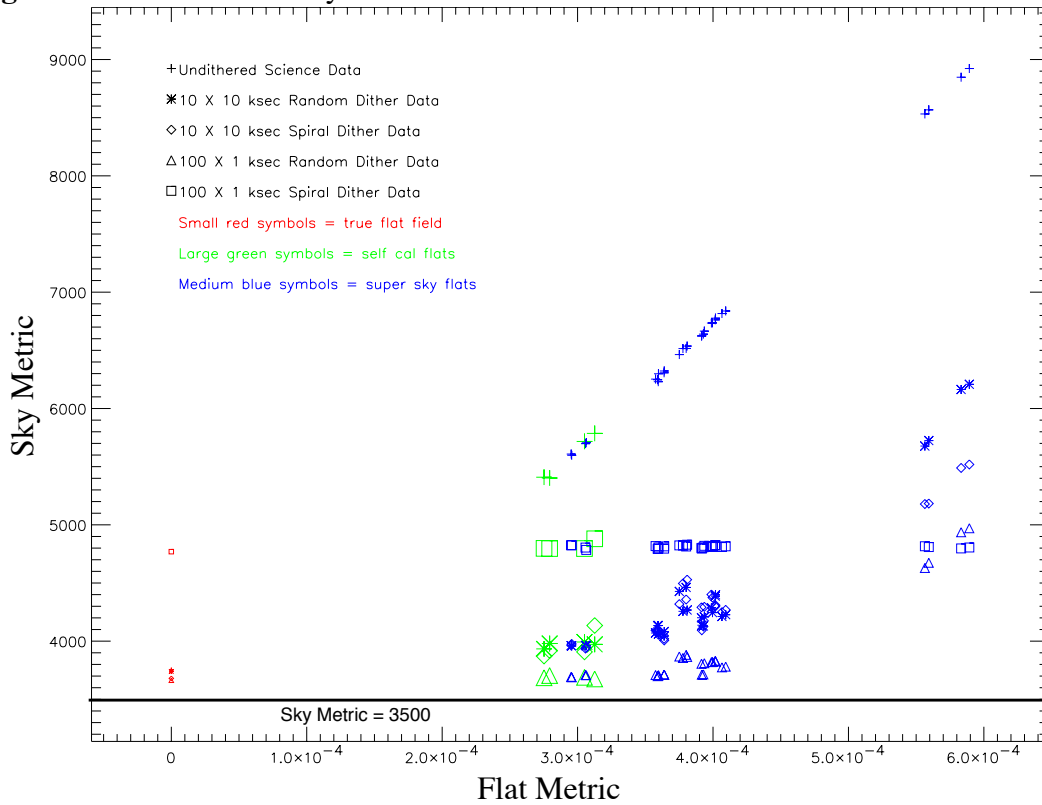


Table 6. Noise metrics for 2 micron science datasets as a function of applied flat field.

Characteristics of Applied Flat Field		2 micron Science Data Noise Metric				
Flat Type	Flat Data	^a No Dither 1 × 100ksec	^b Random 10 × 10ksec	^c Spiral 10 × 10ksec	^d Random 100 × 1ksec	^e Spiral 100 × 1ksec
true flat	N/A	1.00281	1.00130	0.99683	0.971045	0.99612
self-calibration	10 × 10 ksec random	1.52118	1.07103	1.06009	0.97870	1.00568
self-calibration	10 × 10 ksec spiral	1.50820	1.05750	1.07010	0.97781	1.00472
self-calibration	100 × 1 ksec random	1.41423	1.04667	1.04419	0.98031	1.00421
self-calibration	100 × 1 ksec spiral	1.41185	1.04671	1.04689	0.98013	1.00539
3 σ mean super-sky	10 × 10 ksec random dither	1.78214	1.17313	1.19776	1.13581	1.00427
3 σ mean super-sky	10 × 10 ksec spiral dither	2.07457	1.31901	1.36676	1.28429	1.01253
3 σ mean super-sky	10 × 10 ksec chopped	2.03783	1.51383	1.47699	1.67014	1.01230
3 σ mean super-sky	20 × 5 ksec chopped	1.59286	1.12891	1.11056	1.01064	1.00312
3 σ mean super-sky	100 × 1 ksec random dither	10.12780	7.65402	7.92622	5.87787	1.39514
3 σ mean super-sky	100 × 1 ksec spiral dither	2.09685	1.36629	1.44291	1.28887	1.02538
3 σ mean super-sky	100 × 1 ksec chopped	1.66760	1.15799	1.16116	1.07536	1.00395
3 σ median super-sky	10 × 10 ksec random dither	1.83369	1.15969	1.18155	1.10477	1.00725
3 σ median super-sky	10 × 10 ksec spiral dither	2.08115	1.28225	1.31726	1.21957	1.01269
3 σ median super-sky	10 × 10 ksec chopped	1.98804	1.38012	1.36771	1.48852	1.01229
3 σ median super-sky	20 × 5 ksec chopped	1.73390	1.12329	1.11701	1.00173	1.00904
3 σ median super-sky	100 × 1 ksec random dither	9.16517	6.79944	7.02429	5.08244	1.29058
3 σ median super-sky	100 × 1 ksec spiral dither	2.14198	1.33757	1.41593	1.25617	1.02190
3 σ median super-sky	100 × 1 ksec chopped	1.78256	1.14249	1.14296	1.04168	1.00375
5 σ mean super-sky	10 × 10 ksec random dither	1.78181	1.17578	1.19735	1.13429	1.00511
5 σ mean super-sky	10 × 10 ksec spiral dither	2.07824	1.31990	1.37067	1.28174	1.00959
5 σ mean super-sky	10 × 10 ksec chopped	2.02593	1.50584	1.46785	1.64202	1.01225
5 σ mean super-sky	20 × 5 ksec chopped	1.59344	1.12930	1.11462	1.01343	1.00743
5 σ mean super-sky	100 × 1 ksec random dither	10.09780	7.63494	7.90985	5.86196	1.39172
5 σ mean super-sky	100 × 1 ksec spiral dither	2.10643	1.36978	1.46067	1.28463	1.02800
5 σ mean super-sky	100 × 1 ksec chopped	1.66505	1.15647	1.16357	1.07661	1.00476
5 σ median super-sky	10 × 10 ksec random dither	1.84331	1.16322	1.18612	1.11879	1.00985
5 σ median super-sky	10 × 10 ksec spiral dither	2.09640	1.29172	1.32827	1.23859	1.01300
5 σ median super-sky	10 × 10 ksec chopped	2.00278	1.39839	1.37285	1.49083	1.00774
5 σ median super-sky	20 × 5 ksec chopped	1.71948	1.12567	1.11932	1.00316	1.00794
5 σ median super-sky	100 × 1 ksec random dither	9.13247	6.77787	7.00411	5.06730	1.28460
5 σ median super-sky	100 × 1 ksec spiral dither	2.12483	1.33013	1.40572	1.24782	1.02402
5 σ median super-sky	100 × 1 ksec chopped	1.78801	1.14758	1.14338	1.04765	1.00893

^a Includes all 40,000 sky pixels, each with a cumulative exposure time of 100 ksec.

^b Includes 16,157 sky pixels, each with a cumulative exposure time of 100 ksec.

^c Includes 18,422 sky pixels, each with a cumulative exposure time of 100 ksec.

^d Includes 6,141 sky pixels, each with a cumulative exposure time of 100 ksec.

^e Includes 4,967 sky pixels, each with a cumulative exposure time of 60 ksec.

Table 7. Noise metrics for 20 micron science datasets as a function of applied flat field.

Characteristics of Applied Flat Field		20 micron Science Data Noise Metric				
Flat Type	Flat Data	^a No Dither 1 × 100ksec	^b Random 10 × 10ksec	^c Spiral 10 × 10ksec	^d Random 100 × 1ksec	^e Spiral 100 × 1ksec
true flat	N/A	1.00287	0.99915	0.98326	0.97512	1.01331
self-calibration	10 × 10 ksec random	1.55971	1.11466	1.09277	1.03402	1.05102
self-calibration	10 × 10 ksec spiral	1.60976	1.14937	1.18912	1.06429	1.10300
self-calibration	100 × 1 ksec random	1.51109	1.14094	1.15562	1.08025	1.08148
self-calibration	100 × 1 ksec spiral	1.49850	1.12670	1.10717	1.05790	1.06907
3σ mean super-sky	10 × 10 ksec random dither	1.76933	1.30719	1.22320	1.14943	1.05168
3σ mean super-sky	10 × 10 ksec spiral dither	1.78324	1.28525	1.27070	1.14537	1.06458
3σ mean super-sky	10 × 10 ksec chopped	1.81412	1.21089	1.25384	1.19194	1.05629
3σ mean super-sky	20 × 5 ksec chopped	1.70218	1.22440	1.22294	1.23464	1.05330
3σ mean super-sky	100 × 1 ksec random dither	2.38517	1.83497	1.71588	2.02093	1.02097
3σ mean super-sky	100 × 1 ksec spiral dither	1.49765	1.05775	1.06315	0.98229	1.02701
3σ mean super-sky	100 × 1 ksec chopped	1.55674	1.14343	1.13478	1.12111	1.04418
3σ median super-sky	10 × 10 ksec random dither	1.81706	1.23633	1.17321	1.08427	1.03582
3σ median super-sky	10 × 10 ksec spiral dither	1.81455	1.22357	1.20110	1.07863	1.03904
3σ median super-sky	10 × 10 ksec chopped	1.84448	1.19095	1.21648	1.14227	1.04539
3σ median super-sky	20 × 5 ksec chopped	1.79983	1.19925	1.19643	1.17451	1.04882
3σ median super-sky	100 × 1 ksec random dither	2.28566	1.71075	1.64293	1.87934	1.03034
3σ median super-sky	100 × 1 ksec spiral dither	1.67443	1.08829	1.09587	0.98703	1.02745
3σ median super-sky	100 × 1 ksec chopped	1.70888	1.15080	1.12789	1.08856	1.04137
5σ mean super-sky	10 × 10 ksec random dither	1.75383	1.29340	1.20853	1.13992	1.05133
5σ mean super-sky	10 × 10 ksec spiral dither	1.77959	1.28741	1.26557	1.15057	1.06494
5σ mean super-sky	10 × 10 ksec chopped	1.80180	1.20728	1.25182	1.19031	1.05103
5σ mean super-sky	20 × 5 ksec chopped	1.70994	1.23457	1.23234	1.25355	1.05722
5σ mean super-sky	100 × 1 ksec random dither	2.36564	1.84684	1.73700	2.04649	1.01975
5σ mean super-sky	100 × 1 ksec spiral dither	1.50223	1.05882	1.06231	0.98305	1.02824
5σ mean super-sky	100 × 1 ksec chopped	1.55189	1.13692	1.12912	1.11295	1.04611
5σ median super-sky	10 × 10 ksec random dither	1.82009	1.23750	1.17440	1.07863	1.03456
5σ median super-sky	10 × 10 ksec spiral dither	1.81513	1.21337	1.19468	1.07668	1.03825
5σ median super-sky	10 × 10 ksec chopped	1.85006	1.19285	1.21839	1.14105	1.04593
5σ median super-sky	20 × 5 ksec chopped	1.80008	1.19092	1.19973	1.16702	1.04728
5σ median super-sky	100 × 1 ksec random dither	2.29622	1.72573	1.65166	1.89758	1.03031
5σ median super-sky	100 × 1 ksec spiral dither	1.68939	1.08771	1.08947	0.98787	1.02780
5σ median super-sky	100 × 1 ksec chopped	1.70607	1.14360	1.13540	1.09008	1.03843

^a Includes all 40,000 sky pixels, each with a cumulative exposure time of 100 ksec.

^b Includes 13,189 sky pixels, each with a cumulative exposure time of 100 ksec.

^c Includes 18,476 sky pixels, each with a cumulative exposure time of 100 ksec.

^d Includes 5,427 sky pixels, each with a cumulative exposure time of 100 ksec.

^e Includes 4,889 sky pixels, each with a cumulative exposure time of 60 ksec.

Figure 6: Flat metric vs. noise metric for 2 micron science datasets.

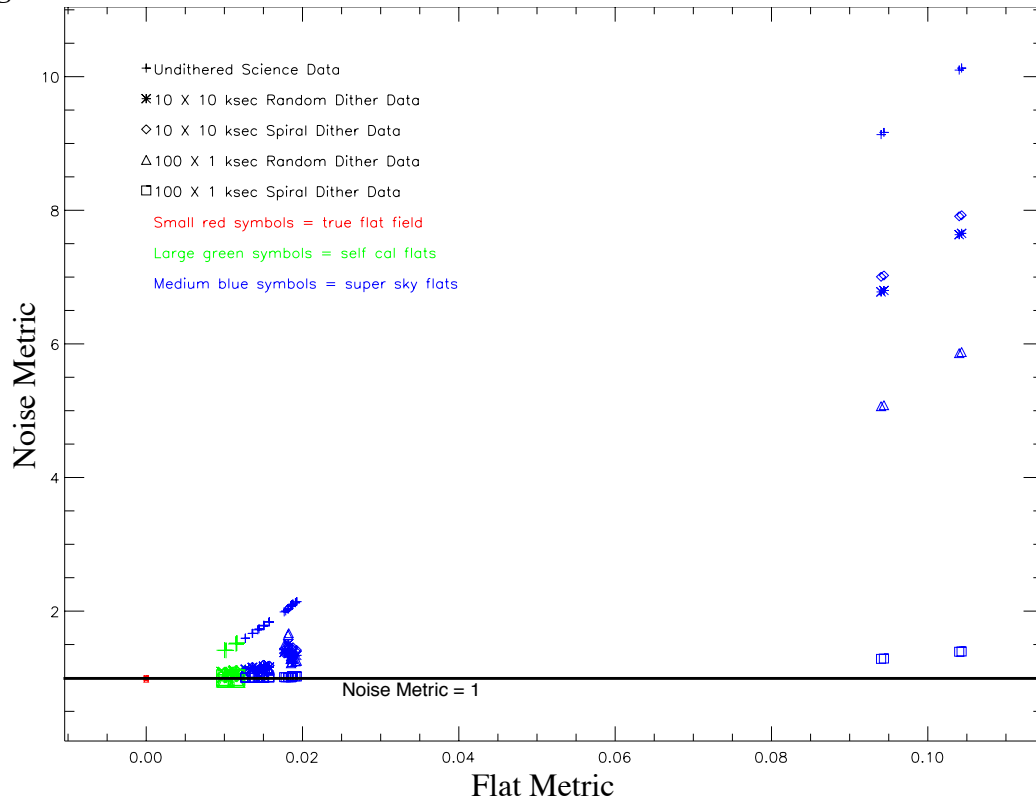
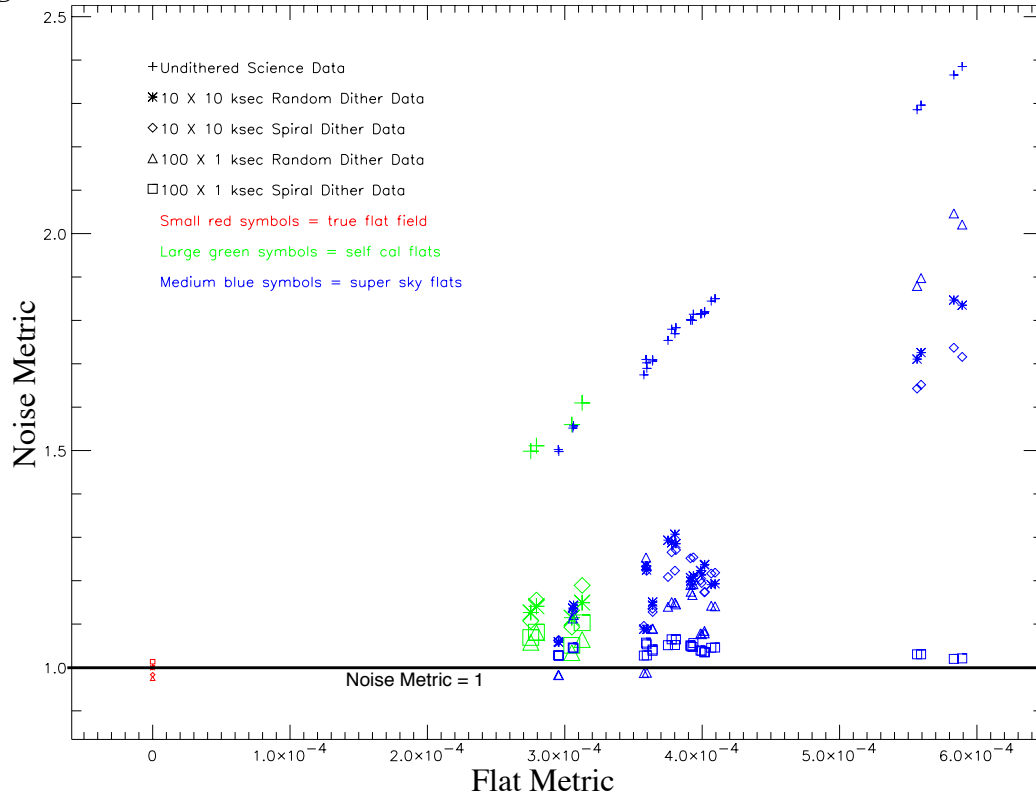


Figure 7: Flat metric vs. noise metric for 20 micron science datasets.



Results

The effects of dithering on the sky metric and noise metrics are illustrated in Table 8 and Table 9, in which the mean and standard deviations of the sky metrics and noise metrics per flat type are given as a function of the number of dither positions in the science data. Flat fields derived from the 100×1 ksec random dither dataset have been excluded. On average, both the mean and the standard deviation of the sky metrics for a given type of flat field improve with the number of dither positions. The noise metrics exhibit the same behavior but the standard deviation of the noise metrics does not. These results emphasize the importance of dithering in order to “beat down the noise” in science observations.

Table 8. Mean & Standard Deviation of Sky Metrics Per Flat Type as a Function of the Number of Science Data Dither Positions.

# Dither Positions in Science Data	Sky Metric Statistics							
	All Flats ^a		Self-Cal Flats		3 σ Super-Sky Flats ^a		5 σ Super-Sky Flats ^a	
	Mean	σ	Mean	σ	Mean	σ	Mean	σ
2 microns								
1	228.77	38.90	174.77	6.37	236.81	34.26	238.73	35.92
10	137.91	25.88	107.96	2.36	143.61	23.12	142.20	26.45
100	113.08	8.25	107.20	0.20	114.00	8.76	114.11	8.69
20 microns								
1	6584.38	930.06	5578.59	201.49	6730.04	925.55	6395.84	396.85
10	4338.09	538.35	3964.06	80.00	4186.97	168.24	4178.97	162.30
100	3886.64	361.55	3688.46	12.28	3768.13	70.44	3765.90	66.53

^a Excludes flat fields derived from 100×1 ksec random dither data.

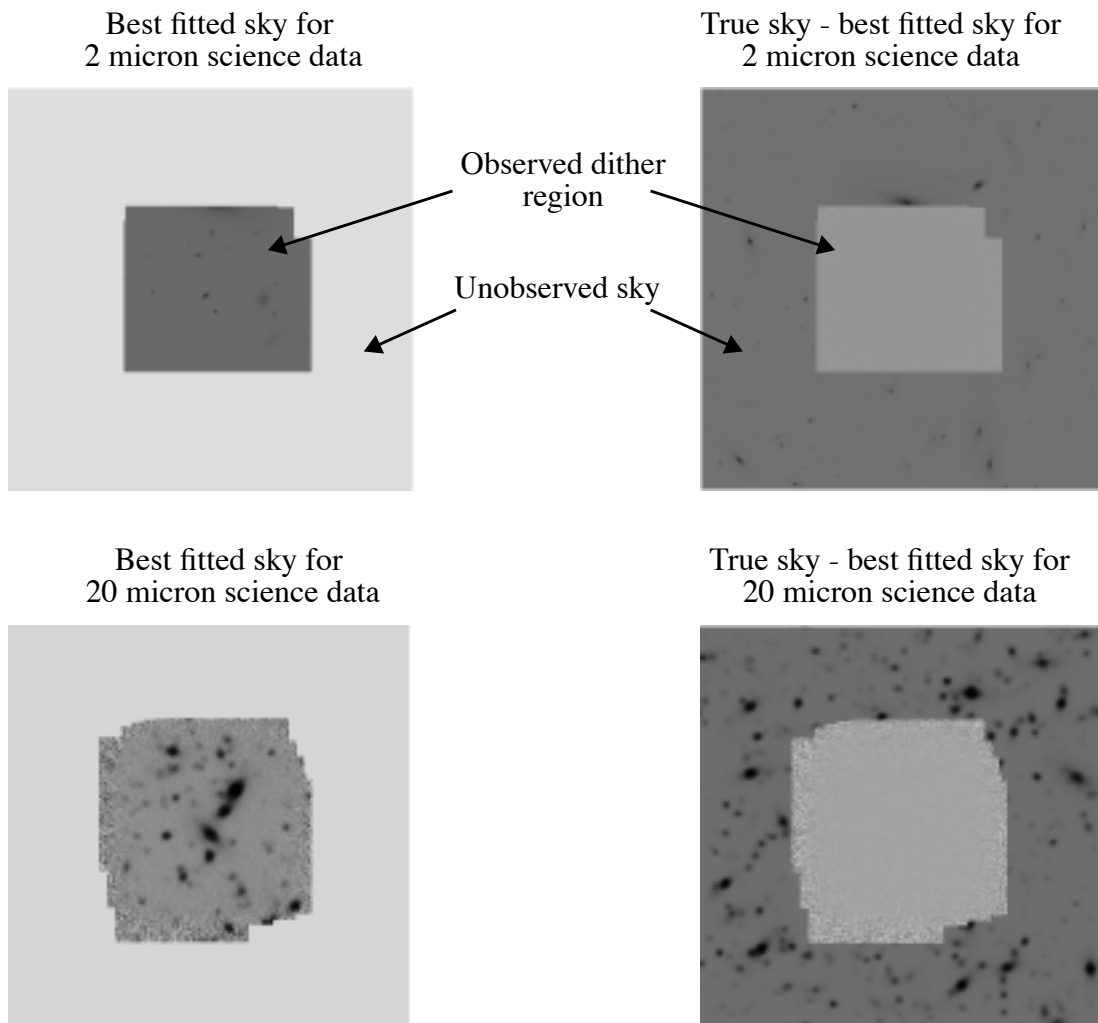
Table 9. Mean & Standard Deviation of Noise Metrics Per Flat Type as a Function of the Number of Science Data Dither Positions.

# Dither Positions in Science Data	Noise Metric Statistics							
	All Flats ^a		Self-Cal Flats		3 σ Super-Sky Flats ^a		5 σ Super-Sky Flats ^a	
	Mean	σ	Mean	σ	Mean	σ	Mean	σ
2 microns								
1	1.839	0.233	1.464	0.059	1.901	0.190	1.902	0.191
10	1.237	0.140	1.055	0.011	1.266	0.129	1.268	0.129
100	1.181	0.198	0.979	0.001	1.215	0.202	1.215	0.195
20 microns								
1	1.705	0.120	1.545	0.051	1.732	0.110	1.732	0.108
10	1.179	0.065	1.134	0.031	1.187	0.068	1.185	0.067
100	1.107	0.073	1.059	0.019	1.115	0.076	1.114	0.078

^a Excludes flat fields derived from 100×1 ksec random dither data.

The best case resulting fitted (calibrated) sky for both the 2 and 20 micron science data is shown in Figure 8. Also shown in the figure are the difference images (true sky - fitted sky). One can see that the flat fields did an excellent job in calibrating the simulated science data; the difference images show virtually no residual sources within the dither regions.

Figure 8: Best case fitted sky and (true sky - fitted sky) for simulated 2 and 20 micron science data. Virtually no residual sources remain in the difference images within the dither region.



Conclusions

This study confirmed the primary finding of CH02, namely, that both the self-calibration and super-sky flat methods are capable of providing flat fields adequate to support JWST science goals.

Super-sky flats derived from datasets containing 10-100 exposures with total exposure times of 100 ksec were found to be good to 1.6% at 2 microns and 0.04% at 20 microns. Self-calibration flat fields, derived from a subset of the datasets used to construct the super-sky flats, were found to be better than the super-sky flats and were good to 1.1% at 2 microns and 0.03% at 20 microns.

Super-sky flats based on the mean of the iteratively sigma-clipped data were comparable to flats based on the median of the clipped data. No systematic differences were found in comparing super-sky flats clipped at the 3σ and 5σ levels.

At 2 microns, self-calibration flat fields resulted in the lowest sky metrics for all 5 science datasets and the best noise metrics for 4 out of 5 datasets. At 20 microns, 4 of the best 5 sky metrics were obtained using self-calibration flats while all of the best noise metrics were from super-sky flats.

Dithering the science data was found to be crucial in obtaining satisfactory calibrations, regardless of the origin of the applied flat field. Both sky metric and noise metric improves with the number of dither positions in the science data. The flat field noise dominates the shot noise in the calibration process, especially at 2 microns.

References

- Arendt, R., Fixsen, R., and Moseley, H. 2000, ApJ 536, 500.
- Casertano, S. 2001, NGST Calibration Overview, STScI-NGST-R-0014 A.
- Casertano, S. and Holfeltz, S. T. 2002 Comparison of Super-Sky and Self-Calibration Flat Fields for Simulated Mid-Infrared JWST Images, STScI-JWST-R-2002-0004 Issue A.
- Fixsen, D., Arendt R., and Moseley, H. 2000, ApJS 128, 651